Title
Fully integrated optical coherence tomography, ultrasound, and indocyanine green-based fluorescence tri-modality system for intravascular imaging.

Journal
Biomedical Optics Express, 8(2)

ISSN
2156-7085

Authors
Li, Yan
Jing, Joseph
Qu, Yueqiao
et al.

Publication Date
2017-02-01

DOI
10.1364/boe.8.001036

Research Article | Vol. 8, No. 2 | 1 Feb 2017 | BIOMEDICAL OPTICS EXPRESS 1036
Biomedical Optics EXPRESS

Fully integrated optical coherence tomography, ultrasound, and indocyanine green-based fluorescence tri-modality system for intravascular imaging

YAN LI,[1] JOSEPH JING,[1] YUEQIAO QU,[1] YUSI MIAO,[1] BUYUN ZHANG,[1] TENG MA,[2] MINGYUE YU,[2] QIFA ZHOU,[2] AND ZHONGPING CHEN[1,3,*]

[1]*Department of Biomedical Engineering and Beckman laser institute, University of California, Irvine, Irvine, CA 92617, USA*
[2]*The Resource Center for Medical Ultrasonic Transducer Technology, University of Southern California, Los Angeles 90089, USA*
[3]*Department of Biomedical Engineering, University of California, 5200 Engineering Hall, Irvine, California 92697, USA*
[*]*z2chen@uci.edu*

Abstract: We present a tri-modality imaging system and fully integrated tri-modality probe for intravascular imaging. The tri-modality imaging system is able to simultaneously acquire optical coherence tomography (OCT), ultrasound (US), and fluorescence imaging. Moreover, for fluorescence imaging, we used the FDA-approved indocyanine green (ICG) dye as the contrast agent to target lipid-loaded macrophages. We conducted imaging from a male New Zealand white rabbit to evaluate the performance of the tri-modality system. In addition, tri-modality images of rabbit aortas were correlated with hematoxylin and eosin (H&E) histology to check the measurement accuracy. The fully integrated miniature tri-modality probe, together with the use of ICG dye suggest that the system is of great potential for providing a more accurate assessment of vulnerable plaques in clinical applications.

OCIS codes: (110.4190) Multiple imaging; (110.4500) Optical coherence tomography; (110.7170) Ultrasound; (170.0170) Medical optics and biotechnology; (170.2150) Endoscopic imaging; (260.2510) Fluorescence.

References and links

1. E. Falk, P. K. Shah, and V. Fuster, "Coronary Plaque Disruption," Circulation **92**(3), 657–671 (1995).
2. A. V. Finn, M. Nakano, J. Narula, F. D. Kolodgie, and R. Virmani, "Concept of Vulnerable/Unstable Plaque," Arterioscler. Thromb. Vasc. Biol. **30**(7), 1282–1292 (2010).
3. M. Naghavi, P. Libby, E. Falk, S. W. Casscells, S. Litovsky, J. Rumberger, J. J. Badimon, C. Stefanadis, P. Moreno, G. Pasterkamp, Z. Fayad, P. H. Stone, S. Waxman, P. Raggi, M. Madjid, A. Zarrabi, A. Burke, C. Yuan, P. J. Fitzgerald, D. S. Siscovick, C. L. de Korte, M. Aikawa, K. E. Airaksinen, G. Assmann, C. R. Becker, J. H. Chesebro, A. Farb, Z. S. Galis, C. Jackson, I. K. Jang, W. Koenig, R. A. Lodder, K. March, J. Demirovic, M. Navab, S. G. Priori, M. D. Rekhter, R. Bahr, S. M. Grundy, R. Mehran, A. Colombo, E. Boerwinkle, C. Ballantyne, W. Insull, Jr., R. S. Schwartz, R. Vogel, P. W. Serruys, G. K. Hansson, D. P. Faxon, S. Kaul, H. Drexler, P. Greenland, J. E. Muller, R. Virmani, P. M. Ridker, D. P. Zipes, P. K. Shah, and J. T. Willerson, "From vulnerable plaque to vulnerable patient: a call for new definitions and risk assessment strategies: Part II," Circulation **108**(15), 1772–1778 (2003).
4. J. A. Ambrose, M. A. Tannenbaum, D. Alexopoulos, C. E. Hjemdahl-Monsen, J. Leavy, M. Weiss, S. Borrico, R. Gorlin, and V. Fuster, "Angiographic progression of coronary artery disease and the development of myocardial infarction," J. Am. Coll. Cardiol. **12**(1), 56–62 (1988).
5. H. M. Garcia-Garcia, M. A. Costa, and P. W. Serruys, "Imaging of coronary atherosclerosis: intravascular ultrasound," Eur. Heart J. **31**(20), 2456–2469 (2010).
6. G. J. Tearney, H. Yabushita, S. L. Houser, H. T. Aretz, I. K. Jang, K. H. Schlendorf, C. R. Kauffman, M. Shishkov, E. F. Halpern, and B. E. Bouma, "Quantification of macrophage content in atherosclerotic plaques by optical coherence tomography," Circulation **107**(1), 113–119 (2003).
7. J. G. Fujimoto, S. A. Boppart, G. J. Tearney, B. E. Bouma, C. Pitris, and M. E. Brezinski, "High resolution in vivo intra-arterial imaging with optical coherence tomography," Heart **82**(2), 128–133 (1999).

#279803 http://dx.doi.org/10.1364/BOE.8.001036
Journal © 2017 Received 1 Nov 2016; revised 6 Jan 2017; accepted 16 Jan 2017; published 24 Jan 2017

Biomedical Optics EXPRESS

8. M.A. Calfon, A. Rosenthal, G. Mallas, A. Mauskapf, R.N. Nudelman, V. Ntziachristos, F.A. Jaffer, "In vivo near infrared fluorescence (NIRF) intravascular molecular imaging of inflammatory plaque, a multimodal approach to imaging of atherosclerosis," J. Vis. Exp. **54**, e2257 (2011).
9. M. Abran, B.E. Stähli, N. Merlet, T. Mihalache-Avram, M. Mecteau, E. Rhéaume, D. Busseuil, J.C. Tardif, F. Lesage, "Validating a bimodal intravascular ultrasound (IVUS) and near-infrared fluorescence (NIRF) catheter for atherosclerotic plaque detection in rabbits," Biomed Opt Express **6**(10), 3989–3999 (2015).
10. S. Lee, M. W. Lee, H. S. Cho, J. W. Song, H. S. Nam, D. J. Oh, K. Park, W. Y. Oh, H. Yoo, and J. W. Kim, "Fully integrated high-speed intravascular optical coherence tomography/near-infrared fluorescence structural/molecular imaging in vivo using a clinically available near-infrared fluorescence-emitting indocyanine green to detect inflamed lipid-rich atheromata in coronary-sized vessels," Circ. Cardiovasc. Interv. **7**(4), 560–569 (2014).
11. Y. Li, X. Gong, C. Liu, R. Lin, W. Hau, X. Bai, and L. Song, "High-speed intravascular spectroscopic photoacoustic imaging at 1000 A-lines per second with a 0.9-mm diameter catheter," J. Biomed. Opt. **20**(6), 065006 (2015).
12. S. Sethuraman, S. R. Aglyamov, J. H. Amirian, R. W. Smalling, and S. Y. Emelianov, "Intravascular photoacoustic imaging using an IVUS imaging catheter," IEEE Trans. Ultrason. Ferroelectr. Freq. Control **54**(5), 978–986 (2007).
13. G. J. Ughi, J. Verjans, A. M. Fard, H. Wang, E. Osborn, T. Hara, A. Mauskapf, F. A. Jaffer, and G. J. Tearney, "Dual modality intravascular optical coherence tomography (OCT) and near-infrared fluorescence (NIRF) imaging: a fully automated algorithm for the distance-calibration of NIRF signal intensity for quantitative molecular imaging," Int. J. Cardiovasc. Imaging **31**(2), 259–268 (2015).
14. Y. Yang, X. Li, T. Wang, P. D. Kumavor, A. Aguirre, K. K. Shung, Q. Zhou, M. Sanders, M. Brewer, and Q. Zhu, "Integrated optical coherence tomography, ultrasound and photoacoustic imaging for ovarian tissue characterization," Biomed. Opt. Express **2**(9), 2551–2561 (2011).
15. S. Liang, T. Ma, J. Jing, X. Li, J. Li, K. K. Shung, Q. Zhou, J. Zhang, and Z. Chen, "Trimodality imaging system and intravascular endoscopic probe: combined optical coherence tomography, fluorescence imaging and ultrasound imaging," Opt. Lett. **39**(23), 6652–6655 (2014).
16. M. Abran, G. Cloutier, M. H. Cardinal, B. Chayer, J.-C. Tardif, and F. Lesage, "Development of a photoacoustic, ultrasound and fluorescence imaging catheter for the study of atherosclerotic plaque," IEEE Trans. Biomed. Circuits Syst. **8**(5), 696–703 (2014).
17. C. Vinegoni, I. Botnaru, E. Aikawa, M. A. Calfon, Y. Iwamoto, E. J. Folco, V. Ntziachristos, R. Weissleder, P. Libby, and F. A. Jaffer, "Indocyanine green enables near-infrared fluorescence imaging of lipid-rich, inflamed atherosclerotic plaques," Sci. Transl. Med. **3**(84), 84ra45 (2011).
18. J. Li, T. Ma, D. Mohar, E. Steward, M. Yu, Z. Piao, Y. He, K. K. Shung, Q. Zhou, P. M. Patel, and Z. Chen, "Ultrafast optical-ultrasonic system and miniaturized catheter for imaging and characterizing atherosclerotic plaques in vivo," Sci. Rep. **5**, 18406 (2015).
19. Z. Piao, T. Ma, J. Li, M. T. Wiedmann, S. Huang, M. Yu, K. K. Shung, Q. Zhou, C. S. Kim, and Z. Chen, "High speed intravascular photoacoustic imaging with fast optical parametric oscillator laser at 1.7 mum," Appl. Phys. Lett. **107**, 083701 (2015).

1. Introduction

Cardiovascular disease is the leading cause of death in developed countries and ruptured atherosclerotic plaques are the main cause of acute coronary events. Identifying plaque type helps the diagnosis and plays an important role in choosing proper interventional techniques. Therefore, accurate assessment of plaque is critical in the clinic. According to clinical studies, three characteristics of plaques are used as the criteria to estimate the presence of vulnerable plaques, which are (1) large lipid pool, (2) thin fibrous cap, and (3) major inflammatory reaction [1–4]. Various imaging techniques, including X-ray angiography, computed tomography (CT) angiography, and magnetic resonance angiography (MRA) have been developed to assess the coronary arteries. However, accurate characterization of plaques with these technologies remains challenging. So far, intravascular imaging is regarded as the most accurate method for characterizing plaques in vivo. In the clinic, intravascular ultrasound (IVUS) can image both the lumen geometry and structure of the arterial wall with an imaging depth of ~7 mm and a resolution of ~150 μm, which can be used to image large lipid pools [5]. On the other hand, intravascular optical coherence tomography (IVOCT) offers a superior spatial resolution of ~15 μm, which has enabled the detection of thin fibrous caps [6,7]. Near-infrared fluorescence imaging is able to obtain specific molecular information by using different contrast agents. For intravascular imaging, near-infrared fluorescence (NIRF) imaging can be used to identify inflammatory reaction, which is one of the main characteristics of vulnerable plaques [8]. However, most imaging systems focus on one or

Biomedical Optics EXPRESS

dual-modality imaging [9–13,18,19], which are not enough for an accurate characterization of these characteristics (large lipid pool, thin fibrous cap, and major inflammatory reaction). For example, it is difficult to identify whether there is a thin fibrous cap or not by using a combined NIRF and IVUS system. Recently, a few tri-modality imaging systems have been reported [14–16], and these works represent a significant step forward for the estimation of atherosclerotic plaques. However, the tri-modality system [14] that combined OCT, US, and photoacoustic (PA) can only obtain imaging by moving the probe instead of rotating, and thus the system cannot truly perform endoscopic imaging such as intravascular imaging. Moreover, the diameter of the probe presented in this study is 5 mm, which is too big to achieve intravascular imaging. Another tri-modality system [15] that combined OCT, US, and fluorescence was also reported from our group. This system is able to get tri-modality intravascular imaging simultaneously. However, the diameter of the probe used in this system is around 1.2 mm, which is still too big for clinical applications. Furthermore, for fluorescence imaging, Cy5.5 dye has been applied as a contrast agent in that work. Cy 5.5 dye is not FDA-approved, which impedes the clinical translation of this technology. For the tri-modality system [16], only phantom experiments were conducted, so the performance of the imaging plaque is unknown. In addition, the imaging speed of PA is relatively lower (~1 frame per 13 seconds) for clinical application.

For accuracy assessment of plaques, it is critical to obtain all the information of the main characteristics of vulnerable plaques. In our study, we developed a tri-modality system with a fully integrated miniature probe. We have reduced the diameter of the probe to 1.06 mm. When inserted in a catheter sheath, it has an outer diameter of 1.3 mm, which is small enough to fit in a 5 French introducer. The system is able to acquire OCT, US, and fluorescence imaging simultaneously. US imaging has a large penetration depth and can be used for identifying the lipid pool. The high-resolution OCT can contribute to the identification of the thin fibrous cap. For fluorescence imaging, FDA-approved ICG dye is used as a contrast agent to indicate the local accumulation of macrophages, which normally corresponds to inflammatory reaction [17]. Ex vivo experiments of rabbit aortas were performed to validate the performance of our tri-modality system. H&E histology results of the rabbit aorta were also presented to check assessment accuracy.

2. Methods

2.1 System design

In order to obtain OCT, US, and fluorescence images, the three imaging technologies need to be fully integrated. In our study, we applied a trigger signal from the swept source laser as the main trigger to synchronize the US and fluorescence imaging. In addition, a wavelength division multiplexer was used to combine the OCT and fluorescence imaging systems. For the fluorescence imaging system, we used a double clad fiber (DCF) coupler (Thorlabs, DC1300LEB) to collect the emission light instead of a free space optical path, which enabled a compact and stable tri-modality system. Figure 1 illustrates the overall setup of the tri-modality system, which consists of a 1310 nm- swept-source OCT (SS-OCT) system, ultrasound imaging system, and fluorescence imaging system. For OCT, the swept source (Santec, HSL- 2100) with a center wavelength of 1310 nm and a sweeping rate of 20 kHz was used. For fluorescence imaging, a 785-nm semi-conductive CW laser (IS785-50 IR, Meshtel) was used as the excitation source, which corresponds to the excitation peak of ICG, and a DCF coupler was incorporated to transmit excitation light and collect emission light. For transmission, the combined beams went through the single mode core of the DCF from port A to port S, and the small diameter of the single mode core contributes to high fluence on surface tissue, which enables a high efficiency excitation. The emission light came back from the first clad of the DCF and core (port S) to a multimode fiber (port B) whose larger diameter and higher NA enhance the capability of collecting emission light, which was filtered by a bandpass filter of 814 to 851 nm (Semrock, Rochester, NY), and then detected

Biomedical Optics EXPRESS

by a photomultiplier tube (PMT, Hamamatsu, Photosensor module: H10722-20). The beams of the SS-OCT and laser diode were combined with a custom-made wavelength division multiplexer (Thorlabs: WDM coupler785/1310). For ultrasound imaging, a JSR Ultrasonics DPR500 DUAL Pulser/Receiver was used to generate and detect ultrasound signal.

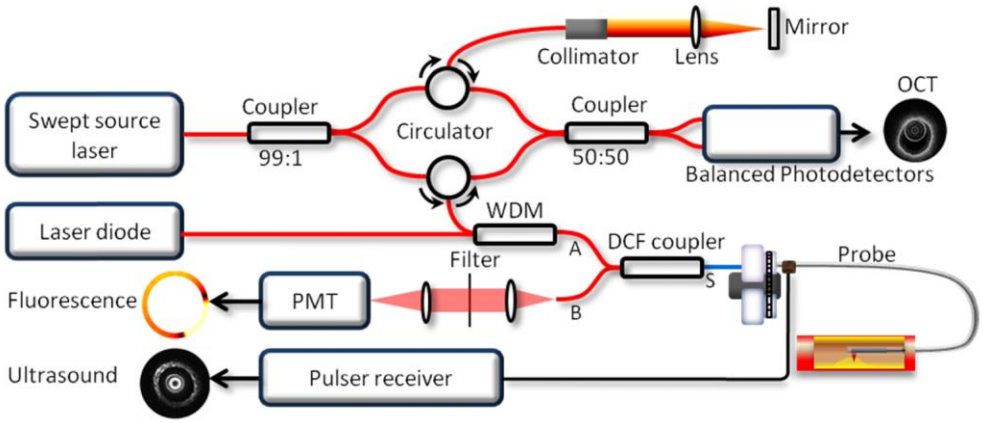

Fig. 1. Overall design of the tri-modality system. WDM: wavelength division multiplexer. PMT: photomultiplier tube. DCF coupler: double clad fiber coupler.

For data acquisition, in consideration of three channels (OCT, US and fluorescence), two synchronized data acquisition cards (Alazar Technologies Inc.,Canada) were used. The C + + program is able to display OCT, ultrasound, and fluorescence imaging in real-time using GPU.

2.2 Imaging probe

For tri-modality imaging, we designed and implemented a fully integrated miniature probe, as shown in Fig. 2(a). The combined beams propagate through the single mode core of the DCF, focused by a 0.5 mm GRIN lens, reflected by a rod mirror (Aviation Magneto Optical Sensor Corp) with a diameter of 0.5 mm at an angle of 43°, then to the tissue surface. The spot size at a 1.5 mm working distance (1310 nm) is around 20 μm. A custom-made single-element ultrasonic transducer (dimension: 0.4 × 0.4 × 0.4 mm) with a center frequency of 40 MHz was sequentially aligned with the optical components and tilted at a slight angle in order to obtain optimum overlap between the optical beams and ultrasound, which contributes to obtaining colocalized tri-modality images. All the elements were housed in a metal cap and fixed by epoxy. The cap was connected to a double-wrapped torque coil (ASAHI INTECC USA). The outer diameter of the element was 1 mm. A custom-made DCF rotary joint was used to propagate the two optical beams and a slip ring was used to deliver electronic signals while rotating the probe. Two motors were used for driving the rotating/pullback catheter assembly. The pullback speed was set to be 1 mm per second with a frame rate of 20 images per second.

We imaged the target at the different distances to acquire basic performance characterizations of the developed probe. For OCT images, the sensitivity, lateral resolution, and depth range are 115 dB, 25μm, and 3-5 mm, respectively. For US images, sensitivity, lateral resolution, and depth range are 72 dB, 200 μm, and 5-6 mm, respectively. For fluorescence images, the minimum concentration of ICG that can be identified is 0.01μmol/L under 5-mW laser power, and lateral resolution and depth range are 30 μm and 3-5 mm, respectively.

Biomedical Optics EXPRESS

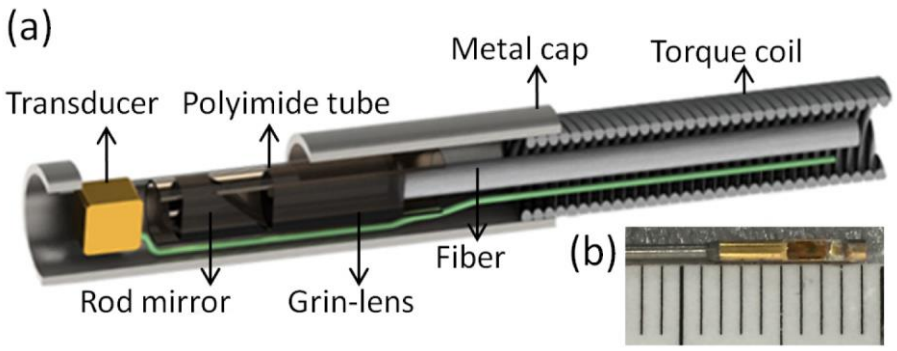

Fig. 2. Tip of the tri-modality probe. (a) Overall schematics. (b) Top view of the probe.

3. Experimental results

3.1 Phantom experiment

In order to demonstrate the performance of the tri-modality imaging system, a lipid-mimicking phantom was fabricated by injecting 0.1 μmol/L of ICG into a healthy pig artery to stain selective regions with ICG while other areas remained unchanged. Figures 3(I)–(IV) show tri-modality images of the phantom at different sites. Figures 3(Ia)-(IVa), 3(Ib)-(IVb), and 3(Ic)-(IVc) are the combined OCT (inner, SNR: 61 dB) and fluorescence (outer, SNR: 113 dB), ultrasound (SNR: 51 dB), and tri-modality images, respectively. Figure (I),(III) and (IV) show tri-modality images at the sites without injecting ICG. From Figs. 3(Ia), 3(IIIa), and 3(IVa), it can be seen that the signal amplitude of fluorescence is significantly lower and homogenous, corresponding to the sites without ICG. From OCT and ultrasound images, the whole structural and micro-structural information can be obtained. From Fig. 3(IIa), it can be found that, the signal amplitude of fluorescence (indicated by the white arrow) is significantly higher than other regions with no ICG, corresponding to the site with ICG. Figures 4(I) and (II) show the reconstructed 3D tri-modality images. Figure 4(Ia)/4(IIa), 4(Ib)/4(IIb), and 4(Ic)/4(IIc) represent 3D fluorescence, OCT, and ultrasound images. These results demonstrate that the tri-modality system has the capability of getting three modalities images at the same time and same location.

Biomedical Optics EXPRESS

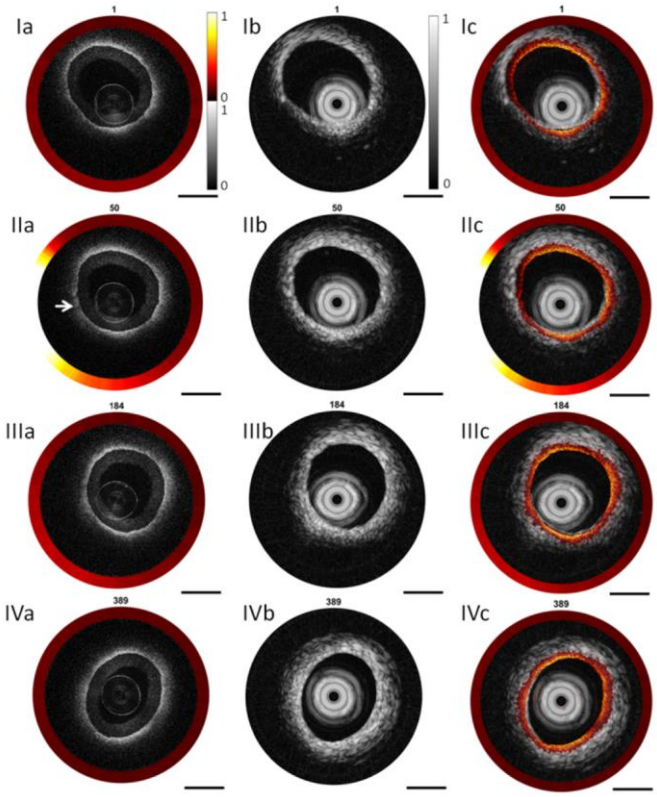

Fig. 3. Tri-modality images of lipid-mimicking phantom. (Ia-IVa) combined OCT (inner) and fluorescence (outer), (Ib-IVb) US, (Ic-IVc) fused tri-modality. The artifact circles in the IVUS images are caused by the ultrasound pulse ring-down effect and the reflection of the catheter sheath. The artifact that is similar to real OCT images but with much lower amplitude is caused by the interference between the target and the interface of the GRIN lens. (I),(III) and (IV) Healthy artery. (II) Healthy artery with ICG. Scale bars are 1 mm.

Biomedical Optics EXPRESS

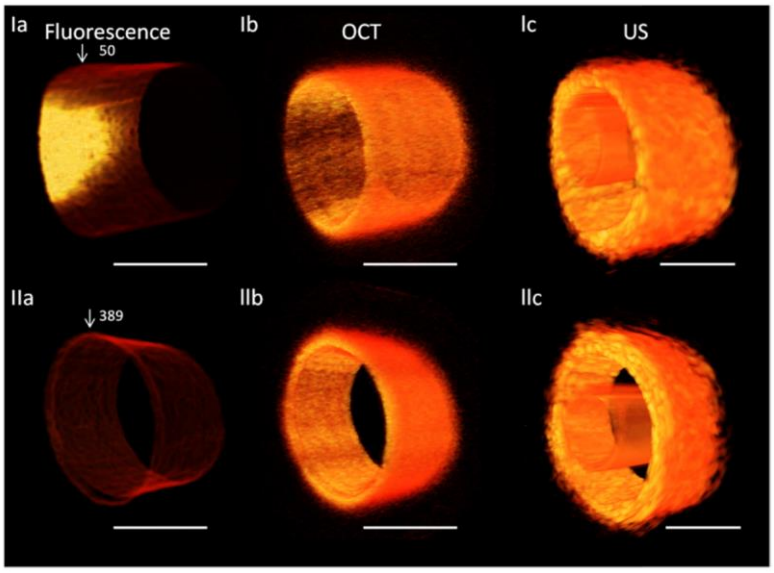

Fig. 4. 3D tri-modality images of lipid-mimicking phantom. (Ia) and (IIa) fluorescence, (Ib) and (IIb) OCT, (Ic) and (IIc) US. Scale bars are 1 mm. The high signal region (in Ia) indicates the existence of ICG.

3.2 Rabbit aorta experiment

To demonstrate the capability of accurately assessing vulnerable plaques, an aorta from an atherosclerotic rabbit was imaged. First, lesions were created by balloon injury and 16 weeks of high-cholesterol diets in a male New Zealand white rabbit, and lesions were similar to those of human atherosclerotic plaques. Then the experimental rabbit was anesthetized and ICG (2.25mg/Kg) was injected. Twenty minutes after injection, the rabbit was sacrificed. The aorta was excised and conserved in 4% formaldehyde for ex vivo experiments.

Representative OCT (SNR: 63 dB), IVUS (SNR: 50 dB), and fluorescence images (SNR: 84 dB) and corresponding H&E staining of coronary artery segments with different pathological features are shown in Fig. 5. IVUS is used as the first step for identifying plaque since IVUS enables the visualization of the layered structures of the artery wall. Due to low soft-tissue contrast, it only provides initial identification of the lipid plaque. Fibrosis and the lipid pool can be differentiated by OCT images based on the its relatively higher soft tissue contrast. Inflammatory region can be identified by fluorescence images to further characterize the stability of the plaque.

From Figs. 5(IIb) and 5(IIIb), intimal thickening and a low-density acoustic signal region (denoted by the white arrow) can be found, which demonstrates the existence of plaque. At the same site in the OCT image [in Fig. 5(IIIa))], a homogenous high signal region also indicates intimal thickening. Moreover, the high signal region is also found at the same site in the fluorescence images, which indicates inflammatory reaction. From the combined tri-modality images, it can be concluded that this aorta as shown in Fig. 5(III) is in the early stage of plaque formation. The classification of plaque type is validated by the corresponding histology photos, which match the tri-modality images well. From Fig. 5(IIa), the diffuse boundary and weak signal region under the high signal region indicates the existence of lipid pool. The thickness of the fiber cap is 150 μm according to Fig. 5(IIA). Furthermore, the high signal at the same site in the fluorescence images indicates an inflammatory reaction. A lipid pool can be found in the corresponding H&E histology photo, which agrees with tri-modality images well. Therefore, we can conclude that the arota shown in Fig. 5(IIa) is Thick-cap (>65 μm) fibroatheroma (ThCFA) in the stage of plaque progression. In Fig. 5(Ib), some low echo

Biomedical Optics EXPRESS

signals can be found, which means that this region may have plaque. However, based on the combined OCT and fluorescence results, it can be concluded that this aorta is normal. Histology further supports this conclusion. From Fig. 5(IV), the tri-modality images and the H&E histology all show that this aorta is healthy. These images and H&E histology illustrate the capability of the tri-modality system to determinate the plaque type. 3D OCT, US, and ICG-based fluorescence images are shown in Fig. 6.

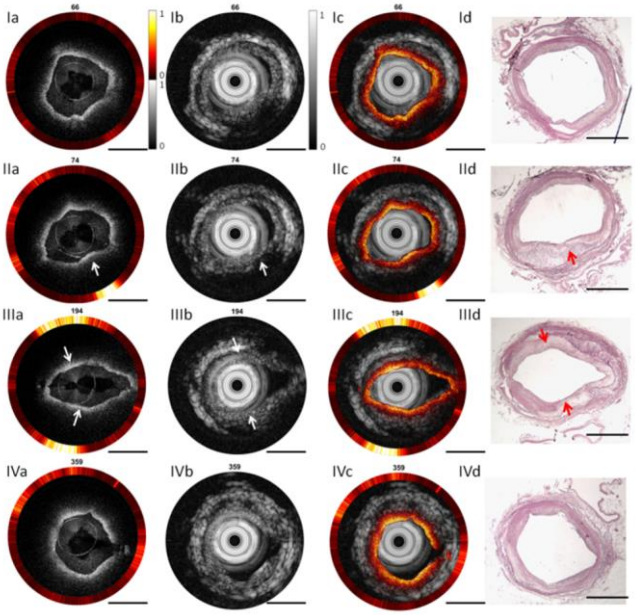

Fig. 5. Tri-modality images of atherosclerotic rabbit . (Ia-IVa) combined OCT (inner) and fluorescence (outer), (Ib-IVb) US, (Ic-IVc) fused tri-modality and (Id-IVd) hematoxylin and eosin(H&E) histology. The artifact circles in the IVUS images are caused by the ultrasound pulse ring-down effect and the reflection of the catheter sheath. (II) and (III) aorta with plaque, indicated by white arrows. (I) and (IV) are healthy aorta. Scale bars are 1 mm.

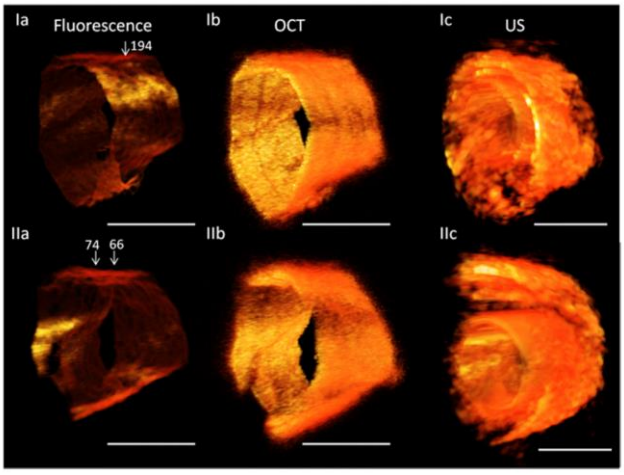

Fig. 6. 3D tri-modality images of atherosclerotic rabbit. (Ia) and (IIa) Fluorescence, (Ib) and (IIb) OCT, (Ic) and (IIc)US. Scale bars are 1 mm.

Biomedical Optics EXPRESS

4. Discussion

In this paper, a tri-modality imaging system with a fully integrated tri-modality intravascular probe was presented. The system has the capability of simultaneously obtaining OCT, ultrasound, and fluorescence data and displaying images in real-time. The diameter of the probe is 1mm, which means that it has great potential for clinical applications. This system may lead to a more accurate assessment of vulnerable plaques. Both phantom and ex-vivo experiment demonstrate that this tri-modality system is capable of obtaining a high-resolution OCT cross-section, deep-penetration ultrasound structure, and molecular-specific ICG-based fluorescence images. Furthermore, H&E staining validated the ex-vivo results. The initial results have shown that the tri-modality system has potential for plaque detection and characterization. The tri-modality system and fully integrated tri-modality imaging probes, in the near future, make the identification of lipid-rich, inflamed plaques that are likely to rupture possible and provide a powerful tool for clinical management of cardiovascular diseases.

Funding

National Institutes of Health (R01HL-125084, R01HL-127271, R01EY-026091, R01EY-021529, and P41EB-015890); Air Force Office of Scientific Research (FA9550-14-1-0034).

Acknowledgments

The authors gratefully acknowledge Mr. E. Steward, Mr. D. Mohar, Ms. R. Khedraki, and Mr. A. Naqvi for their assistance during surgical procedures.